Journal of Power Sources 660 (2025) 238544

Contents lists available at ScienceDirect

Journal of Power Sources

journal homepage: www.elsevier.com/locate/jpowsour

Suppressing internal short circuit caused thermal runaway of lithium-ion batteries through current modulation

Siyi Liu [a,1], Madeline Liu [a,1], Mary K. Long [a], Muriel Carter [a], Nolan Brugler [a], Guangsheng Zhang [a,*], Chao-Yang Wang [b,**]

[a] Department of Mechanical & Aerospace Engineering, The University of Alabama in Huntsville, Huntsville, AL, 35899, USA
[b] Electrochemical Engine Center (ECEC) and Department of Mechanical Engineering, The Pennsylvania State University, University Park, PA, 16802, USA

HIGHLIGHTS

- A novel strategy of suppressing battery thermal runaway is demonstrated.
- Without current modulation Al-Anode ISC and Al-Cu ISC triggered thermal runaway.
- With proper current modulation thermal runaway was prevented in both cases.
- *In situ* diagnosis, energy balance, and post-mortem analysis revealed the mechanism.
- The strategy works by minimizing local heating and promoting uniform heating.

GRAPHICAL ABSTRACT

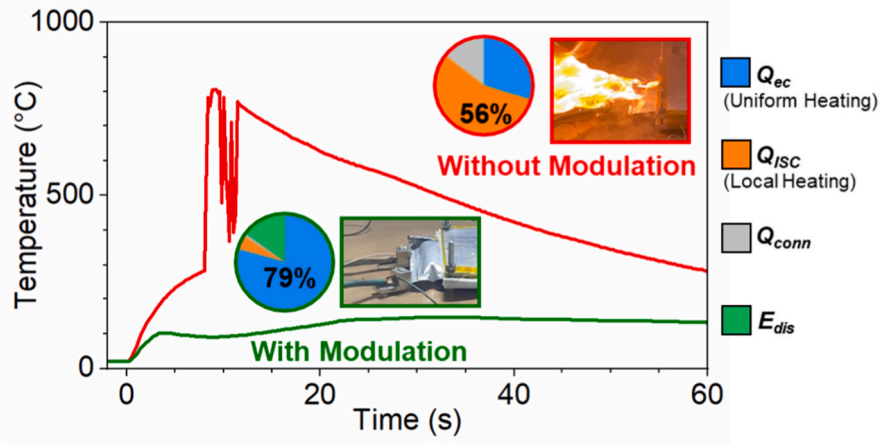

ARTICLE INFO

Keywords:
Li-ion battery
Internal short circuit
Thermal runaway suppression
Current modulation
In situ diagnosis
Energy balance analysis

ABSTRACT

We report a current modulation strategy that suppresses internal short circuit (ISC)-caused thermal runaway of Li-ion cells. The strategy works by guiding current flow outside a cell in the event of a serious ISC to reduce local internal heating. Using 4-Ah cells with NMC811 cathode and graphite anode, and a reliable ISC triggering and quantification method, we demonstrated that thermal runaway would start within a few seconds of Al-Anode ISC or Al-Cu ISC without current modulation. In comparison, thermal runaway was effectively suppressed with proper current modulation. Quantification through *in situ* diagnosis showed that current modulation reduced heat generation at the ISC location by an order of magnitude and reduced the maximum temperature dramatically. Further energy balance analysis and post-mortem analysis supported the hypothesis that the strategy of current modulation works by minimizing local heating and promoting uniform heating.

* Corresponding author.
** Corresponding author.
E-mail addresses: gz0002@uah.edu (G. Zhang), cxw31@psu.edu (C.-Y. Wang).
[1] These authors contributed equally.

https://doi.org/10.1016/j.jpowsour.2025.238544
Received 23 August 2025; Received in revised form 22 September 2025; Accepted 29 September 2025

1. Introduction

Thermal runaway of energy-dense batteries, particularly lithium-ion (Li-ion) batteries, has been a critical challenge for decades [1]. The challenge becomes increasingly urgent with the proliferation of large-format Li-ion batteries for electric vehicles (EVs) and grid-scale energy storage systems [2,3]. Thermal runaway can be caused not only by abuse conditions (thermal, electrical, and mechanical) but also by non-abuse internal short circuit (ISC) [4]. ISC-caused thermal runaway is especially concerning and intriguing because it can occur even when the batteries are in normal use or during open circuit [3,5]. Many high-profile and costly spontaneous Li-ion battery fires have been attributed to ISC-caused thermal runaway, involving various applications such as smart phones [6], EVs [5,7], airplanes [8], and energy storage systems [9].

Tremendous efforts and progress have been made in suppressing thermal runaway [10,11], such as emergency cooling [12], phase change materials (PCM)-based cooling [13], polymer-substrate current collectors [14,15], temperature-responsive switching materials between electrodes and current collectors [16–18], fire retardant additives in electrolyte [19], and solid state electrolytes [20]. However, each strategy has its drawbacks due to the competing requirements for safety, energy density, power performance, durability, and cost of batteries [2,21–24]. For example, emergency cooling and PCM-based cooling could lower the energy density of battery packs [2]. Polymer-substrate current collectors made of thin metal layers coated on polymer substrate could reduce power performance during normal operation. Fire retardant additives in electrolyte could influence the performance and durability. Even all-solid-state batteries with nonflammable solid electrolytes, which are generally expected to be fundamentally safe, can still experience ISC or thermal runaway according to recent calculations of the adiabatic temperature [2,21] and experimental reports [22,24]. Therefore, alternative strategies for the prevention and suppression of battery thermal runaway are still needed.

Inspired by the ancient wisdom in flood control, *dredging and guiding rather than blocking the water* [25], here we report a novel strategy for suppressing ISC-caused thermal runaway based on current modulation. Moreover, through quantification of ISC behaviors, we not only demonstrate the effectiveness of the strategy, but also explain why it works. The strategy is schematically shown in Fig. 1a–c. In a normal Li-ion cell without ISC (Fig. 1a), no electronic current flows through the separator and the risk of thermal runaway is low. If a serious ISC happens in a Li-ion cell (Fig. 1b), a large electronic current can flow through the separator, concentrated at the ISC location, and cause rapid local heating. The local heating can then cause rapid temperature rise and side reactions [26], leading to more heating and temperature rise with a high risk of thermal runaway. If the Li-ion cell with ISC is forced to be externally discharged through current modulation (Fig. 1c), the majority of the electronic current can be guided outside of the cell. Correspondingly, heating at the ISC location can be significantly reduced. Furthermore, the guided discharge can lower the state-of-charge (SOC) of the Li-ion cell. Therefore, the risk of thermal runaway can be dramatically reduced through current modulation.

To test the effectiveness of the proposed current modulation strategy, we first need to trigger and quantify ISC and thermal runaway of Li-ion cells reliably. Note that various methods have been developed to create ISC in Li-ion cells and advanced the understanding of their behaviors [27–33], but many of these methods are unable to precisely control and quantify critical ISC parameters. Consequently, the test results are usually limited to pass-fail statements or qualitative descriptions [34]. Such a lack of quantification hinders the fundamental understanding of ISC behaviors and the development of safer battery technologies. Moreover, repeatability of testing results is a challenge for some methods [18,35]. Our group recently reported a novel method for simultaneous triggering and *in situ* sensing of ISC in Li-ion cells with good repeatability [36]. However, the Li-ion cells in that study did not go to thermal runaway during ISC due to the small ISC current and the small capacity of the cells. The method was improved in this work by using larger ISC pads and higher capacity Li-ion cells with NMC 811 cathode (less stable than NMC622 in the previous study). Based on the improved method, the strategy of suppressing thermal runaway by current modulation is demonstrated and investigated herein using 4-Ah pouch format Li-ion cells with a NMC811 cathode and an artificial graphite anode.

Details of the ISC triggering method, experimental cell fabrication, ISC and current modulation test protocol, and experimental setup are described in Section 2. Then, the experimental results of ISC tests without and with current modulations are presented and discussed in Section 3. Future work is also proposed. Finally, based on the results and discussion, conclusions are made and presented in Section 4.

2. Experimental methods

2.1. Working principles of ISC pad method

As schematically shown in Fig. 2a and b, a pair of Cu pad and Al pad are inserted into a Li-ion cell and then connected outside the cell through a switch and a current sensor. When the switch is closed, electrons flow from the anode (negative electrode) to the cathode (positive electrode), through the Cu pad, the switch, the current sensor, and the Al pad. Meanwhile, lithium ions flow from the anode to the cathode through the separator. The created ISC current and heat generation at the pad location behave similarly to those in Fig. 1b, thus enabling investigation of ISC-caused thermal runaway. Note that the method enables creation of four different types of ISC, as schematically shown in Fig. 2c, by removing part of the cathode coating, the anode coating, or both the cathode and the anode coatings at the ISC location. Supplementary Fig. S1 shows pictures of ISC pads and electrodes in experimental Li-ion cells with different types of ISC. As schematically shown in Fig. 2b and d, the

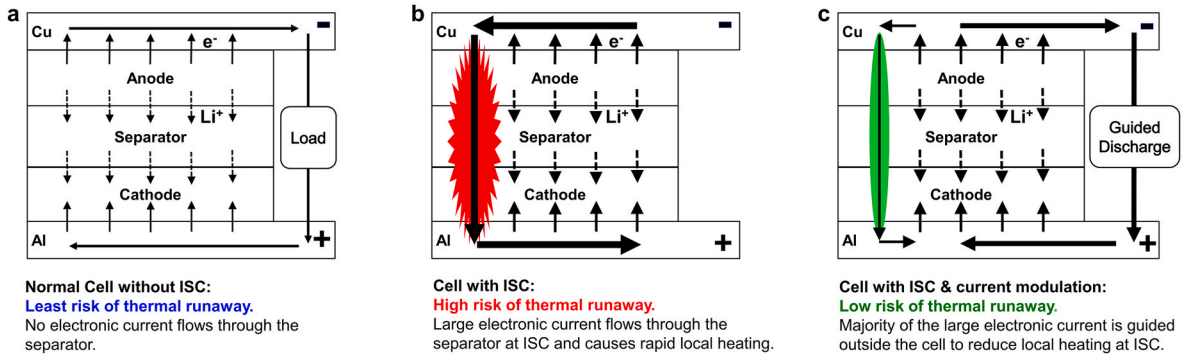

Fig. 1. Strategy of suppressing thermal runaway through current modulation. Schematics of current flows in: **a**, A normal cell without ISC, **b**, A cell with a serious ISC, and **c**, A cell with a serious Al-Cu ISC and current modulation (guided discharge to an external load).

method allows simultaneous measurement of ISC parameters. ISC temperature (T_{ISC}) is measured by embedding a micro temperature sensor between the Cu pad and the Al pad. ISC current (I_{ISC}) is measured directly by the current sensor. ISC resistance on the anode side (R_{NE}) and cathode side (R_{PE}) are obtained by measuring the voltage drops between the cell tabs and the pads (V_{NE} and V_{PE}) and dividing them by the ISC current. With ISC current and ISC resistance known, the ISC heat generation rate can be calculated from $I_{ISC}^2 \bullet (R_{NE} + R_{PE})$. Fig. 2e depicts the experimental connections of a 4-Ah cell with a pair of Cu and Al pads inserted.

2.2. Fabrication of Li-ion cells with embedded ISC triggering pads

Commercially available customized 4-Ah pouch-format dry cells from Li-FUN Technologies (model 7651A0) are used to fabricate experimental cells. Each cell is a full cell and consists of 23 layers of double-side-coated anodes (66 μm in coating thickness of each side) and 22 layers of double-side-coated cathodes (44 μm in coating thickness of each side). The anode active material is artificial graphite (9.5 mg/cm^2, 95.7 % active material) and the cathode active material is NMC811 (14.7 mg/cm^2, 95.5 % active material). The anode and cathode current collectors are copper (8 μm in thickness) and aluminum (12 μm in thickness), respectively. The separator (12 μm in thickness) is polyethylene (PE, 9 μm in thickness) with a special ceramic coating (3 μm in thickness). The area of the anode is 88 mm by 47 mm, and the area of the cathode is 85 mm by 44 mm. The overall thickness of the cell with pouch is ~6.4 mm. The tabs are 12 mm wide and 0.25 mm thick. The mass of the anode layers including copper current collector is ~25 g. The mass of the cathode layers including aluminum current collector is ~27 g. The mass of all of the separator layers is ~2.5 g. The mass of the Al and Cu pads are ~1 g total. The mass of the cell packaging, including tabs, is ~8.5 g.

Each Al pad is made from an Al strip (8 mm wide and 0.09 mm thick, PLiB-ATC8, MTI Corporation). Each Cu pad is made from a Cu strip (8 mm wide and 0.15 mm thick, Amazon). These strips are wider than those in our previous study [36] to enable passage of higher ISC current. To avoid piercing the separators or electrodes by the Al pad and the Cu pad, the corners of the pads at the ISC location are rounded. Additional layers of 0.5-mm Kapton tape is added to the ISC region of each of the pads to ensure stable contact between the pads and electrodes during ISC tests [36]. A K-type micro thermocouple (40 AWG, 5TC-TT-K-40-36-ROHS, Omega Engineering) is taped to a small piece of separator and placed between the ISC pads. Details of how the thermocouples are placed can be seen from Supplementary Fig. S1–3, especially Supplementary Fig. S3b–d.

After inserting the ISC pads and the thermocouple into a dry cell, the cell is partially sealed and then dried in a vacuum oven for at least 8 h. Then, 12 g of electrolyte (1 M LiPF6 in EC + EMC, 3:7 in volume, MTI Corporation) is added to the cell in an argon-filled glovebox (Labstar Pro, MBRAUN) before the cell is completely sealed. An additional K-type thermocouple (5TC-TT-K-40-36-ROHS, Omega Engineering) is attached to the cell surface above the ISC location with a piece of Kapton tape. The total mass of the fabricated cell is ~76 g. Finally, the cell is placed between two layers of ceramic fiber insulation sheet (alumina silica with binder, 1.6 mm thick, McMASTER CARR) and then compressed by a pair of aluminum alloy plates (6061, 6.4-mm thick, McMASTER CARR) with four bolts tightened to 2-Nm torque each. The compression force applied to the cell is ~1200 N as calibrated by a load cell (DYMH-102, 500 kg, CALT). The compression is necessary to ensure good contact between the ISC pads and electrodes/current collectors during ISC tests. The ceramic fiber insulation sheet is used to reduce out-of-plane heat transfer from the cell to the Al alloy compression plates. Supplementary Fig. S2–S3 show details of fabricating Li-ion cells with Al-Cu and Al-Anode ISC, respectively.

2.3. Cell formation and ISC test protocol

After each experimental cell is assembled, the cell goes through a formation process. The cells are held at 1.5 V for 12 h, then charged and discharged at C/20 rate (4.2 V max and 2.8 V min) for one cycle, followed by two more cycles at C/10 rate. Then, the cell is tested at different C rates (C/3, 1C, and 2C) to check its performance. 1C rate refers to the current of 4 A based on the theoretical capacity of 4 Ah.

In each ISC test, the Cu pad and the Al pad were connected outside the cell through a 0.75-mΩ shunt resistor (SHD1-100C075DE, Ohmite) and a relay switch (LEV200A4ANA, Tyco), which was manually controlled through a power supply. To ensure safety, all of the ISC tests were conducted in a safety chamber for battery abuse testing (MSK-TE905, MTI Corporation). Voltage was recorded between the cell-voltage tabs, between the positive voltage tab and the Al pad, between the negative voltage tab and the Cu pad, and between the two pads. Internal and surface temperatures were also recorded. All the data were

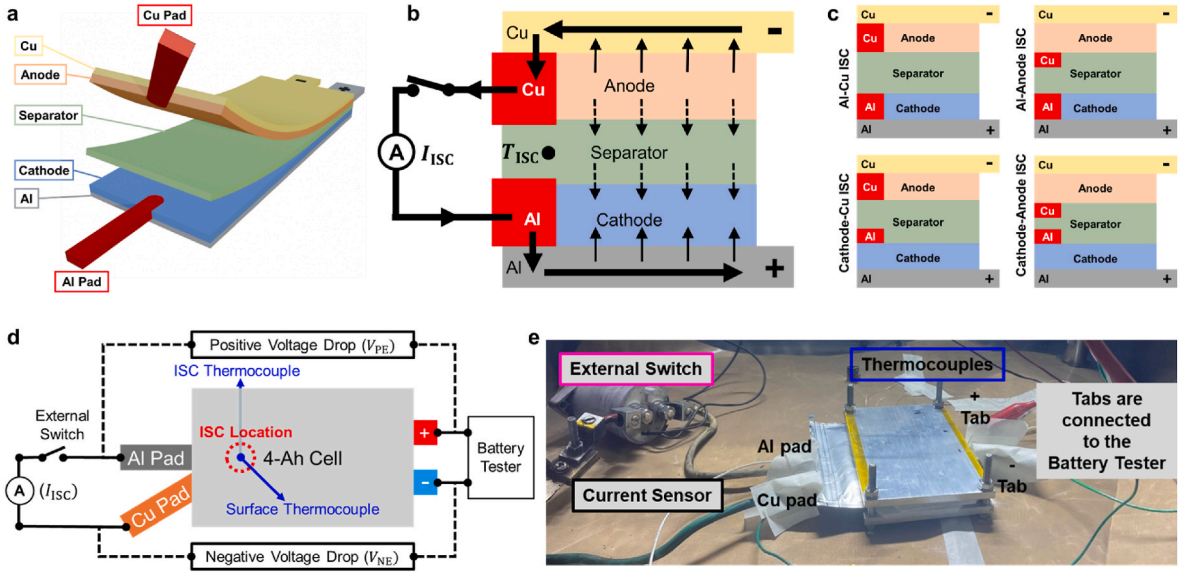

Fig. 2. Method for triggering and quantifying ISC. a, 3D schematic of a cell with embedded ISC pads. **b**, Schematic for on-demand ISC triggering method. **c**, Schematic of different types of ISC. **d,** Schematic of experimental setup. **e**, A picture of experimental setup.

recorded by a data acquisition unit (34980A, Keysight Technologies) at the frequency of 5 Hz. Before each ISC test, the Li-ion cells were fully charged by a battery tester (LBT21084, Arbin) at room temperature (23 ± 2 °C) using a constant current constant voltage (CCCV) protocol (4 A charging until the cell voltage reached 4.2 V, then 4.2 V charging until the current dropped to 0.02 A). For ISC tests with current modulation, the external discharge is implemented by the battery tester and starts when the cell voltage drops to below 4.0 V. For the case of ISC test with simultaneous external short circuit, the external short circuit is implemented by a relay switch (LEV200A4ANA, Tyco) and the external short current is measured by a 0.75-mΩ shunt resistor (SHD1-100C075DE, Ohmite). The total resistance of external short circuit is ~6 mΩ as measured by a high frequency resistance meter (3561, HIOKI). Fig. 2d schematically illustrates these connections and Fig. 2e depicts an image of a cell with all of the connections. Supplementary Fig. S4 compares the C/3 and 2C discharge performance of ISC cells to that of a baseline cell, which is similar. The similarity suggests that the embedded ISC pads have minimum effects on the performance of the experimental Li-ion cells.

2.4. Cell disassembly and SEM imaging

One Li-ion cell with Al-Anode ISC was disassembled for postmortem analysis of the separators after current modulation testing. The cell was fully discharged and then disassembled in an argon-filled glovebox for samples of separators. The separators were washed three times using dimethyl carbonate (DMC, 99 %, Thermo Scientific) and dried before moving out of the glovebox for further examination. Fresh separators from a dry cell were also examined for comparison. The samples were examined using a Thermo Scientific™ Apreo scanning electron microscope (SEM) at The University of Alabama Core Analytical Facility. The separator samples were gold coated using a sputter coater prior to the SEM imaging.

3. Results and discussion

3.1. Triggering and quantification of ISC and thermal runaway

Fig. 3 shows the results of three cells with Al-Anode ISC configuration to demonstrate that this method has good repeatability. Al-Anode ISC is first chosen because an earlier modeling study [37] suggested that Al-Anode ISC has the highest risk of thermal runaway. It can be seen that all the cells went to thermal runaway and behaved very similarly, suggesting that the method has very good repeatability and reliability in triggering ISC and thermal runaway.

Note that the results not only include commonly monitored cell surface temperature and cell voltage, but they also include the ISC temperature, the ISC current, the ISC resistance, and the ISC heat generation rate which are not available in most ISC experimental studies. These additional parameters are helpful in understanding the behaviors of ISC and thermal runaway. For example, the ISC temperature was much more responsive than cell surface temperature. As shown in Fig. 3a, the ISC temperature was nearly 300 °C when thermal runaway started and reached peak values of ~800 °C. In comparison, the surface temperature was only ~50 °C when thermal runaway started, did not indicate thermal runaway until ~2 s later, and reached peak values of less than 600 °C. Unlike the cells in our previous study [36] which did not go to thermal runaway, all three cells in this study went to thermal runaway. Comparison of the results indicated much higher ISC current and ISC heat generation rate for cells in this study. In particular, the ISC current and ISC heat generation rate quickly dropped to less than 30 A in the previous study of 1.5-Ah cells due to mass transport limitation and the rapid decrease of local SOC. In comparison, the 4-Ah cells in this study are able to sustain the large ISC current of ~90A until triggering thermal runaway. This comparison suggests that the Li-ion cell capacity significantly influences the risks of thermal runaway during ISC. Therefore, caution must be exerted when extrapolating findings from small-capacity cells to large-capacity cells in the evaluation of Li-ion cell thermal runaway risk.

It is interesting to note that the ISC current was ~90 A, and took ~10 s to trigger thermal runaway. The total discharged electrochemical energy (E_{ec}) during this period of time would be ~3600 J as determined from Eq. (1):

$$E_{ec} = \int_0^{t_{TR}} I_{ISC} U_0 dt \tag{1}$$

where t_{TR} is the time when thermal runaway starts, and U_0 is the open circuit voltage (assumed to decrease linearly during ISC). If E_{ec} is

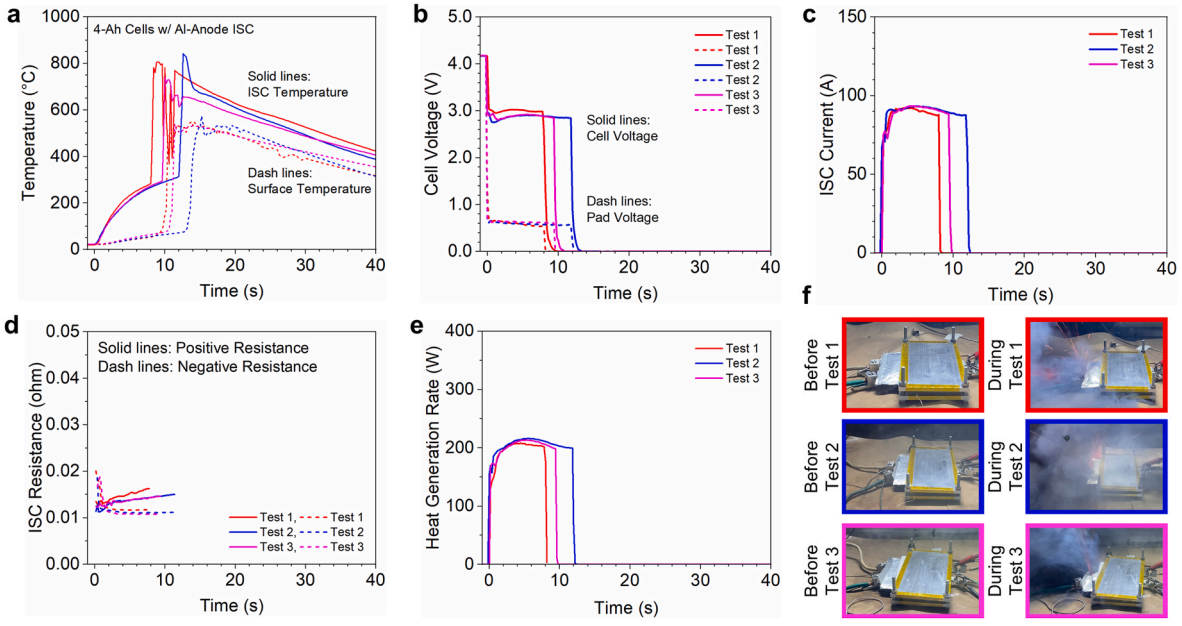

Fig. 3. Reliable triggering of Al-Anode ISC and thermal runaway. a, ISC and cell surface temperature. **b**, Cell voltage. **c**, ISC current. **d**, ISC resistance. **e**, ISC heat generation rate. **f**, Snapshots of cells before and during the tests.

completely converted to thermal energy (assuming no heat loss to the ambient) and heats the cell uniformly, the average temperature rise of the cell (ΔT_{ad}) can be estimated from Eq. (2) [2,23]:

$$\Delta T_{ad} = \frac{E_{ec}}{m_{cell} c_p} \tag{2}$$

where m_{cell} is the cell mass (0.076 kg), and c_p is the specific heat of the cell (assuming 1000 J kg^{-1} K^{-1} [38]). The average temperature rise would only be 48 °C, which is not high enough to trigger thermal runaway. However, the heating in the ISC cells is not uniform and highly concentrated at the ISC location, making the local temperature at the ISC location much higher than the rest of the cell to trigger thermal runaway. This non-uniform heating behavior can be quantified from the following energy balance analysis.

As implied in Fig. 2b, the discharged electrochemical energy during an ISC test (E_{ec}), as defined in Eq. (1) above, is converted into three components. The first is heating associated with the flow of lithium ions and electrochemical reactions (Q_{ec}), which is distributed across the entire cell. The second is ohmic heating at the ISC location due to the electronic current flowing through the ISC pads (Q_{ISC}). The third is ohmic heating due to the electronic current flowing through the connections outside the cell (Q_{conn}), including the switch, the current sensor, and the connecting wires. Therefore, the energy balance can be described by Eq. (3):

$$E_{ec\_no\_modulation} = Q_{ec} + Q_{ISC} + Q_{conn} \tag{3}$$

$E_{ec\_no\_modulation}$ can be estimated from Eq. (1). Q_{ec} can be estimated from Eq. (4) by neglecting reversible heat generation:

$$Q_{ec} = \int_0^{t_{TR}} I_{ISC}(U_0 - V_{cell})dt \tag{4}$$

Q_{ISC} can be estimated from Eq. (5):

$$Q_{ISC} = \int_0^{t_{TR}} I_{ISC}^2 R_{ISC} dt \tag{5}$$

Q_{conn} can be estimated from Eq. (6):

$$Q_{conn} = \int_0^{t_{TR}} I_{ISC}^2 R_{conn} dt \tag{6}$$

Note that t_{TR} is the time when thermal runaway started. Supplementary Table S1 shows the results of the energy balance analysis in the three tests. A significant component of heat generation, ~56 % on average, is concentrated at the ISC location, which would cause the ISC temperature to be much higher than the rest of the cell, consistent with the results in Fig. 3a. Such quantification of local heating clearly reveals the danger of ISC-caused thermal runaway.

Quantification of ISC behaviors is further demonstrated by triggering different types of ISC. As shown in Fig. 4, Al-Cu ISC also led to thermal runaway, while Cathode-Anode ISC and Cathode-Cu ISC did not. The interesting phenomena of Cathode-Anode ISC and Cathode-Cu ISC not triggering thermal runaway can be clearly explained by the quantitative results. Fig. 4d shows that the cathode side ISC resistance is more than 200 times higher than the anode side resistance. Correspondingly, the ISC current is very small, less than 2 A. The small ISC current leads to dramatically smaller heat generation rate and ISC temperature in cells with Cathode-Anode ISC or Cathode-Cu ISC than those with Al-Anode ISC or Al-Cu ISC. In fact, the ISC current and temperature rise are so small that no obvious damage was caused to the cells. As shown in Supplementary Fig. S5 and S6, the Li-ion cells with Cathode-Anode ISC and Cathode-Cu ISC have similar discharge performance before and after the ISC test. In comparison, the ISC currents are much higher in cells with Al-Anode ISC or Al-Cu ISC, which can be attributed to the much lower resistance of Al foil as compared to the cathode.

The lower risk of Cathode-Anode ISC and Cathode-Cu ISC as compared to Al-Anode ISC and Al-Cu ISC has been reported in earlier work through modeling [37] or experiments [39]. However, this work is the first experimental study that directly compares the thermal runaway risk of different types of ISC through quantification of ISC resistance, ISC current, ISC heat generation, and ISC temperature.

The results in Fig. 4 and their comparison with previous studies show that the behaviors and consequences of ISC can be very different depending on the ISC type, ISC resistance, cell capacity, materials, etc. and therefore must be thoroughly examined through quantitative experiments.

3.2. Suppression of thermal runaway through current modulation

After establishing the reliability of triggering thermal runaway by Al-

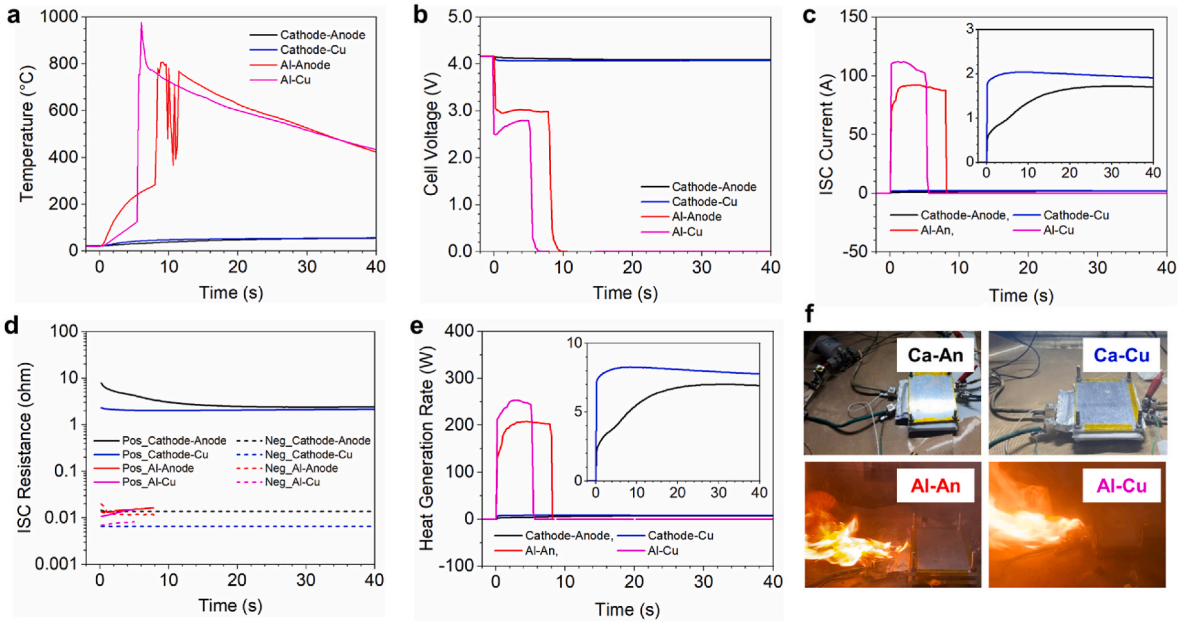

Fig. 4. Results of Li-ion cells with four different types of ISC. a, ISC temperature. **b**, Cell voltage. **c**, ISC current. **d**, ISC resistance. **e**, ISC heat generation rate. **f**, Snapshots of cells during ISC tests.

Anode ISC and Al-Cu ISC, we investigated the effects of the current modulation strategy in suppressing thermal runaway.

The strategy is first applied to cells with Al-Anode ISC using different levels of current modulation: 60 A, 120 A, and external short circuit (ESC). Note that in the 120 A case, the external current is set to be a maximum of 120 A and cell voltage varies between 0.5 V and 0.75 V. As shown in Fig. 5, current modulation using 120 A or ESC successfully prevented thermal runway, with the cells remaining intact after ISC tests as shown in Fig. 5f. Although the 60 A current modulation did not prevent thermal runaway, it postponed the thermal runaway onset time from 10 s to 30 s, which would still be beneficial in practice to activate battery thermal management systems.

As shown in Fig. 5c–e, the effectiveness of the current modulation strategy can be attributed to the dramatically reduced ISC current and heat generation. With 120 A current modulation, the ISC current quickly decreased to ~20 A, much lower than that in the baseline case (~90 A). The decrease of the heat generation rate is even more dramatic, from ~200 W to ~10 W. Consequently, the ISC temperature stayed below 150 °C. These results support the hypothesis schematically shown in Fig. 1c that external current modulation can reduce the ISC current, heat generation, and maximum temperature to suppress thermal runaway.

The effectiveness of the current modulation strategy can be further understood from an energy balance analysis in Eq. (7):

$$E_{ec\_with\_modulation} = Q_{ec} + Q_{ISC} + Q_{conn} + E_{dis} \tag{7}$$

Q_{ISC} and Q_{conn} have the same meaning as in Eq. (3) and can be estimated by Eqs. (5) and (6).

$E_{ec\_with\_modulation}$ in the case of current modulation can be estimated from Eq. (8):

$$E_{ec\_with\_modulation} = \int_0^t (I_{ISC} + I_{ext}) U_0 dt \tag{8}$$

in which I_{ext} is the modulated current flowing outside the cell through the battery tester. Note that in some cases with current modulation, the cells did not go to thermal runaway and therefore the upper time limit cannot be set as t_{TR}. The upper time limit is set to 40 s based on data in Fig. 5.

Q_{ec} in the case of current modulation can be estimated in Eq. (9) by neglecting reversible heat generation:

$$Q_{ec} = \int_0^t (I_{ISC} + I_{ext})(U_0 - V_{cell}) dt \tag{9}$$

E_{dis} refers to the electric energy discharged by the battery tester and can be estimated by Eq. (10):

$$E_{dis} = \int_0^t I_{ext} V_{cell} dt \tag{10}$$

Supplementary Table S2 shows the energy balance analysis results of the different modulation currents. Fig. 6 compares details of the baseline case and the 120 A current modulation case. The ratio of ISC heat generation (Q_{ISC}) to total energy consumption (E_{ec}) is significantly reduced by current modulation. In the case of 120 A, the ratio (only ~5 %), has dropped more than tenfold as compared to the baseline case (~56 %). Correspondently, Q_{ec} became dominant and was distributed throughout the entire cell, leading to uniform heating. This energy balance analysis suggests that the current modulation strategy works not only by reducing ISC heat generation, but also by promoting uniform heat generation.

The strategy of current modulation is then applied to a Li-ion cell with Al-Cu ISC and 120 A guided discharge. As shown in Supplementary Fig. S7, the current modulation also successfully prevented thermal runaway, further confirming the feasibility of suppressing ISC-caused thermal runaway through current modulation. The ISC current was reduced from ~120 A to ~25 A, and the ISC heat generation rate was reduced from ~250 W to ~10 W within 3 s. Energy balance analysis is also performed for the Al-Cu ISC cell. As shown in Supplementary Table S3, the ratio of Q_{ISC} to E_{ec} was reduced from ~54 % to ~6 %, consistent with the cases of Al-Anode ISC.

3.3. Postmortem analysis

Cells with 120 A current modulation were further tested to understand the mechanisms. As shown in Fig. 7a–b, Al-Anode ISC with 120 A current modulation was terminated at 1000 s. The cell voltage quickly recovered to above 3 V and then slowly decreased, indicating the existence of additional minor ISC. Even with additional minor ISC, the cell did not experience thermal runaway. The cell with Al-Cu ISC and current

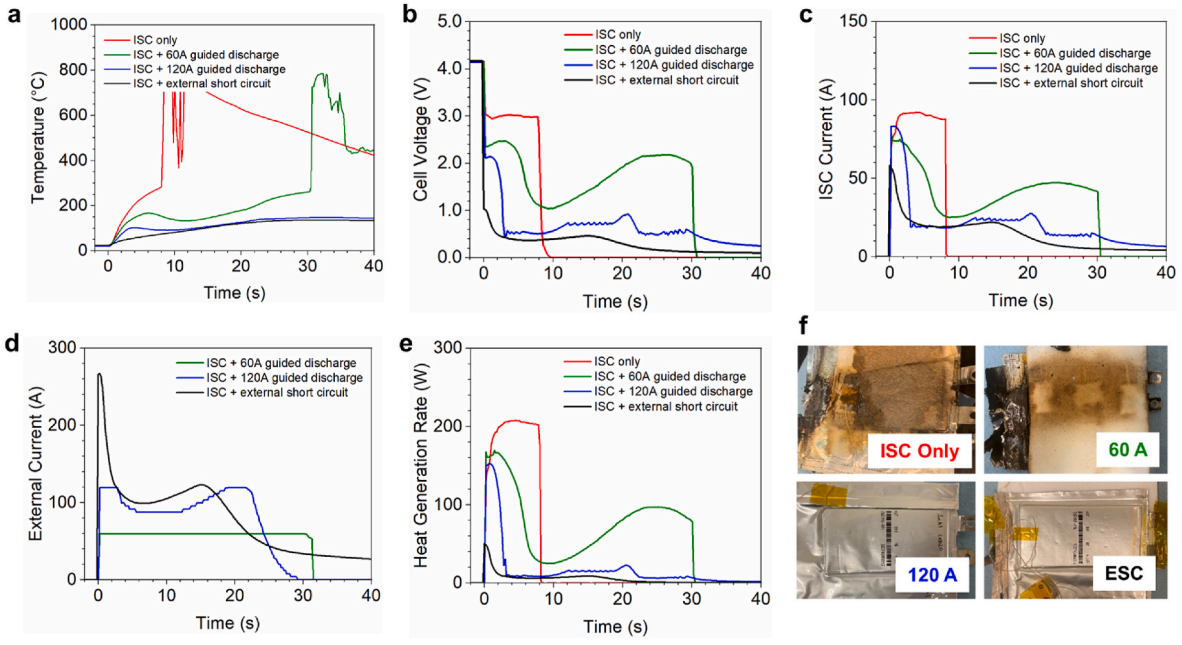

Fig. 5. Effects of different current modulation on Li-ion cells with Al-Anode ISC. a, ISC temperature. **b**, Cell voltage. **c**, ISC current. **d**, External current. **e**, ISC heat generation rate. **f**, Pictures of cells after ISC tests.

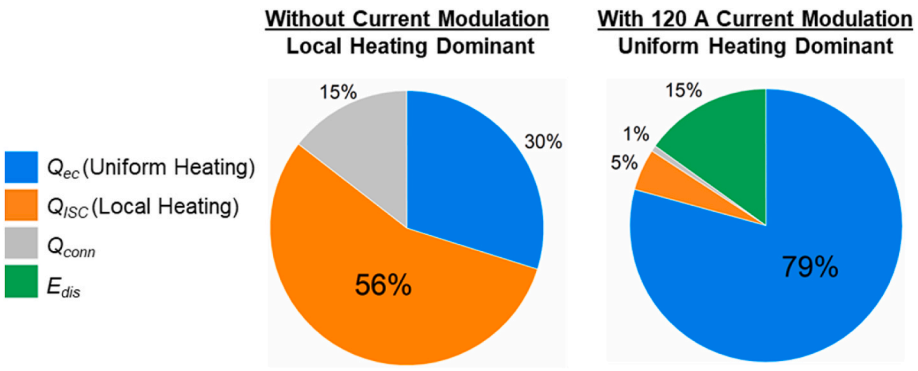

Fig. 6. Energy balance of Al-Anode ISC cells without and with current modulation.

modulation showed similar behaviors (Supplementary Fig. S8). These results indicate that cells with 120 A current modulation failed safely in the events of serious ISC rather than going to thermal runaway as the baseline cell did.

Fig. 7c shows that the cell could not be charged/discharged, indicating that the cell's internal resistance dramatically increased after the ISC and current modulation process. Based on this observation and earlier energy balance analysis, it was hypothesized that current modulation enables uniform heating and safe shutdown of the separator to suppress thermal runaway. To test this hypothesis, a cell with Al-Anode ISC and 120 A current modulation was disassembled for examination of the separators. Fig. 7d–e shows the optical and SEM images of a separator from a fresh dry cell and a separator from the ISC cell, both facing the anode side. The separator pores can be seen in the fresh cell, but are not visible in the ISC cell. This comparison of the SEM images indicates that the separator from the Al-Anode ISC cell with current modulation indeed experienced melting and shutdown. Supplementary Fig. S9 shows separators of additional layers from the same ISC cell, which contain similar observations to Fig. 7e. Note that there are some small particles attached to some regions of the separators in the ISC cell. It would be interesting to determine the chemical composition of these particles and their sources in future work to better understand the melting process during ISC with current modulation. The separator in the cells was polyethylene (PE) based (according to the manufacturer), which has a melting point of ~140 °C [40]. This melting point lies between the ISC and surface temperature (Fig. 7a), providing additional

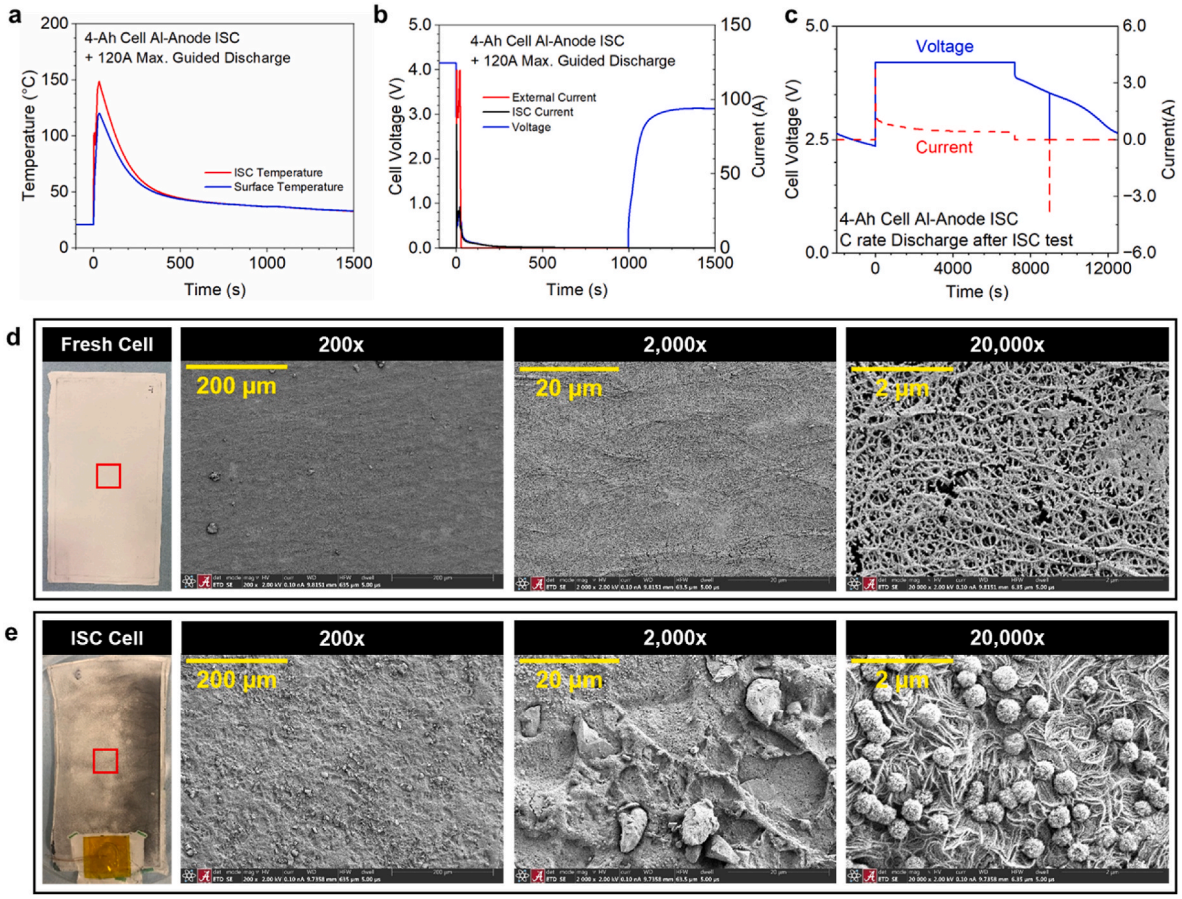

Fig. 7. Characterization of a cell with Al-Anode ISC and 120 A current modulation. a-b, Results of temperature, cell voltage and currents during ISC test. **c**, Cell voltage and current during 1C charging/discharging after ISC test. **d-e**, Optical and SEM images (200x, 2,000x, and 20,000x) of a separator from a fresh dry cell and the Al-Anode ISC cell with current modulation.

evidence of separator melting/shutdown. Supplementary Fig. S10 shows SEM images of the separators facing the cathode side. It can be seen that the cathode side of the separators from the ISC cell do not have any significant difference from the separator in the fresh dry cell due to the heat-resistant ceramic coating layer. This coating layer would prevent the separator from shrinking when the PE-based layer melts, thus preventing major ISC and allowing the separator to shutdown safely. These evidences support the hypothesis that current modulation enables uniform heating of the cell and shutdown of the separator to suppress thermal runaway.

3.4. Future work

More work needs to be done on the strategy of suppressing thermal runaway through current modulation. First, cells in this study are thermally insulated and tested at 100 % SOC, and therefore represent worst-case scenarios as a proof of concept. Cells in actual applications are usually cooled and at various SOC, which could influence the behaviors of ISC and risk of thermal runaway [41,42]. It is therefore helpful to determine and optimize the current modulation depending on cooling conditions and SOC. Second, pouch format 4-Ah single cells are used in this study to demonstrate the effectiveness of the proposed current modulation strategy. The method can be extended to different cell designs (e.g., cylindrical cells, prismatic cells, or cells with polymer-substrate current collectors), capacities, chemistries, and to the module or pack level to optimize the current modulation strategy. The ISC pads are located at the edge of the center layer in this study for the convenience of cell fabrication. They can also be placed at different locations of the cells to characterize ISC behaviors. Third, in this study the current modulation is implemented through a battery tester and starts when the cell voltage drops below 4.0 V due to the start of Al-Anode ISC or Al-Cu ISC as a proof of concept. In practical applications, implementation of the current modulation strategy should be integrated with battery management systems using more sophisticated control algorithm. Fourth, *in situ* characterization of current distribution, temperature distribution, and separator porosity distribution in the cells with and without current modulation will help better understand and optimize the strategy. Ultimately, it is important to determine the critical conditions of thermal runaway during ISC for battery cells with specific designs and operating conditions, and to optimize the current modulation protocols to prevent the battery cells from reaching the critical conditions.

4. Conclusions

We reported a novel strategy for the suppression of ISC-caused thermal runaway of Li-ion cells by guiding electronic current flow outside of Li-ion cells during ISC. The following conclusions can be made. First, we demonstrated a method to reliably trigger and quantify ISC-caused thermal runaway in Li-ion cells. With this method, we showed that both Al-Anode ISC and Al-Cu ISC can trigger thermal runaway in 4-Ah cells, while Cathode-Anode ISC and Cathode-Cu ISC would not trigger thermal runaway due to the high resistance of the cathode. Second, we demonstrated that proper current modulation can suppress ISC-caused thermal runaway, although further optimization is needed. Energy balance analysis revealed that current modulation reduced the fraction of heat generation at the ISC location from above 50 % to ~5 %, while uniform heating associated with electrochemical reactions throughout the cell became dominant. Lastly, post-mortem analysis supported the hypothesis that current modulation enables uniform heating and safe shutdown of the separator.

CRediT authorship contribution statement

Siyi Liu: Writing – review & editing, Writing – original draft, Visualization, Methodology, Investigation, Formal analysis, Data curation. **Madeline Liu:** Writing – review & editing, Writing – original draft, Visualization, Methodology, Investigation, Formal analysis, Data curation. **Mary K. Long:** Writing – review & editing, Methodology. **Muriel Carter:** Writing – review & editing, Visualization, Data curation. **Nolan Brugler:** Writing – review & editing, Data curation. **Guangsheng Zhang:** Writing – review & editing, Writing – original draft, Visualization, Supervision, Resources, Project administration, Methodology, Investigation, Funding acquisition, Formal analysis, Data curation, Conceptualization. **Chao-Yang Wang:** Writing – review & editing, Conceptualization.

Declaration of competing interest

The authors declare the following financial interests/personal relationships which may be considered as potential competing interests: Guangsheng Zhang reports financial support was provided by National Science Foundation. Siyi Liu reports financial support was provided by National Science Foundation. Madeline Liu reports financial support was provided by National Science Foundation. Chao-Yang Wang reports financial support was provided by Diefenderfer Chair endowment. If there are other authors, they declare that they have no known competing financial interests or personal relationships that could have appeared to influence the work reported in this paper.

Acknowledgements

Financial support from the US National Science Foundation under the award # 2240029 is gratefully acknowledged. CY Wang acknowledges the support of Diefenderfer Chair endowment. This work utilized resources (SEM) owned and maintained by the Core Analytical Facility, which is supported by The University of Alabama.

Appendix A. Supplementary data

Supplementary data to this article can be found online at https://doi.org/10.1016/j.jpowsour.2025.238544.

Data availability

Data will be made available on request.

References

[1] M.S. Whittingham, Proc. IEEE 100 (2012) 1518–1534, https://doi.org/10.1109/JPROC.2012.2190170.
[2] R.S. Longchamps, X.-G. Yang, C.-Y. Wang, ACS Energy Lett. 7 (2022) 1103–1111, https://doi.org/10.1021/acsenergylett.2c00077.
[3] J.A. Jeevarajan, T. Joshi, M. Parhizi, T. Rauhala, D. Juarez-Robles, ACS Energy Lett. 7 (2022) 2725–2733, https://doi.org/10.1021/acsenergylett.2c01400.
[4] X. Feng, D. Ren, X. He, M. Ouyang, Joule 4 (2020) 743–770, https://doi.org/10.1016/j.joule.2020.02.010.
[5] R. Aalund, W. Diao, L. Kong, M. Pecht, IEEE Access 9 (2021) 89527–89532, https://doi.org/10.1109/access.2021.3090304.
[6] M. Loveridge, G. Remy, N. Kourra, R. Genieser, A. Barai, M. Lain, Y. Guo, M. Amor-Segan, M. Williams, T. Amietszajew, M. Ellis, R. Bhagat, D. Greenwood, Batteries 4 (2018) 1–11, https://doi.org/10.3390/batteries4010003.
[7] Z. Zhang, H. Dong, L. Wang, Y. Wang, X. He, Energy Technol. (2024) 12, https://doi.org/10.1002/ente.202400931.
[8] NTSB, NTSB Aircraft Incident Report, NTSB/AIR-14/01 PB2014-108867, 2014, http://www.ntsb.gov/investigations/AccidentReports/Reports/AIR1401.pdf.
[9] D. Hill, Battery Energy Storage System Event - Technical Analysis and Recommendations, DNV GL – Document No.: 10209302-HOU-R-01, 2020. https://www.aps.com/en/About/Our-Company/Newsroom/Articles/Equipment-failure-at-McMicken-Battery-Facility.
[10] K. Liu, Y. Liu, D. Lin, A. Pei, Y. Cui, Sci. Adv. 4 (2018) eaas9820, https://doi.org/10.1126/sciadv.aas9820.
[11] D. Ouyang, Y.-H. Chung, J. Liu, J. Bai, Y. Zhou, S. Chen, Z. Wang, C.-M. Shu, Prog. Energy Combust. Sci. 108 (2025) 101209, https://doi.org/10.1016/j.pecs.2025.101209.
[12] P. Qin, Z. Jia, K. Jin, Q. Duan, J. Sun, Q. Wang, J. Power Sources 516 (2021) 230659, https://doi.org/10.1016/j.jpowsour.2021.230659.
[13] X. Dai, D. Kong, J. Du, Y. Zhang, P. Ping, Process Saf. Environ. Prot. 159 (2022) 232–242, https://doi.org/10.1016/j.psep.2021.12.051.

[14] Y. Ye, L.-Y. Chou, Y. Liu, H. Wang, H.K. Lee, W. Huang, J. Wan, K. Liu, G. Zhou, Y. Yang, A. Yang, X. Xiao, X. Gao, D.T. Boyle, H. Chen, W. Zhang, S.C. Kim, Y. Cui, Nat. Energy 5 (2020) 786–793, https://doi.org/10.1038/s41560-020-00702-8.
[15] M.T.M. Pham, J.J. Darst, W.Q. Walker, T.M.M. Heenan, D. Patel, F. Iacoviello, A. Rack, M.P. Olbinado, G. Hinds, D.J.L. Brett, E. Darcy, D.P. Finegan, P. R. Shearing, Cell Rep. Phys. Sci. 2 (2021) 100360, https://doi.org/10.1016/j.xcrp.2021.100360.
[16] Z. Chen, P.-C. Hsu, J. Lopez, Y. Li, J.W.F. To, N. Liu, C. Wang, S.C. Andrews, J. Liu, Y. Cui, Z. Bao, Nat. Energy 1 (2016) 15009, https://doi.org/10.1038/nenergy.2015.9.
[17] W. Ji, F. Wang, D. Liu, J. Qian, Y. Cao, Z. Chen, H. Yang, X. Ai, J. Mater. Chem. A 4 (2016) 11239–11246, https://doi.org/10.1039/C6TA03407A.
[18] I.T. Song, J. Kang, J. Koh, H. Choi, H. Yang, E. Park, J. Lee, W. Cho, Y.M. Lee, S. Lee, N. Kim, M. Lee, K. Kim, Nat. Commun. 15 (2024) 8294, https://doi.org/10.1038/s41467-024-52766-9.
[19] X. Chen, S. Yan, T. Tan, P. Zhou, J. Hou, X. Feng, H. Dong, P. Wang, D. Wang, B. Wang, M. Ouyang, K. Liu, Energy Storage Mater. 45 (2022) 182–190, https://doi.org/10.1016/j.ensm.2021.11.026.
[20] C. Wang, J.T. Kim, C. Wang, X. Sun, Adv. Mater. 35 (2023) e2209074, https://doi.org/10.1002/adma.202209074.
[21] A.M. Bates, Y. Preger, L. Torres-Castro, K.L. Harrison, S.J. Harris, J. Hewson, Joule 6 (2022) 742–755, https://doi.org/10.1016/j.joule.2022.02.007.
[22] R. Chen, A.M. Nolan, J. Lu, J. Wang, X. Yu, Y. Mo, L. Chen, X. Huang, H. Li, Joule 4 (2020) 812–821, https://doi.org/10.1016/j.joule.2020.03.012.
[23] S. Liu, G. Zhang, C.-Y. Wang, ASME J. Heat Mass Transf. 145 (2023) 080801, https://doi.org/10.1115/1.4056823.
[24] S. Ge, T. Sasaki, N. Gupta, K. Qin, R.S. Longchamps, K. Aotani, Y. Aihara, C.-Y. Wang, ACS Energy Lett. 9 (2024) 5747–5755, https://doi.org/10.1021/acsenergylett.4c02564.
[25] Q. Wu, Z. Zhao, L. Liu, D.E. Granger, H. Wang, D.J. Cohen, X. Wu, M. Ye, O. Bar-Yosef, B. Lu, J. Zhang, P. Zhang, D. Yuan, W. Qi, L. Cai, S. Bai, Science 353 (2016) 579–582, https://doi.org/10.1126/science.aaf0842.
[26] X. Feng, M. Ouyang, X. Liu, L. Lu, Y. Xia, X. He, Energy Storage Mater. 10 (2018) 246–267, https://doi.org/10.1016/j.ensm.2017.05.013.
[27] B. Mao, H. Chen, Z. Cui, T. Wu, Q. Wang, Int. J. Heat Mass Tran. 122 (2018) 1103–1115, https://doi.org/10.1016/j.ijheatmasstransfer.2018.02.036.
[28] B. Liu, X. Duan, C. Yuan, L. Wang, J. Li, D.P. Finegan, B. Feng, J. Xu, J. Mater. Chem. A 9 (2021) 7102–7113, https://doi.org/10.1039/d0ta12082k.
[29] F. Ren, T. Cox, H. Wang, J. Power Sources 249 (2014) 156–162, https://doi.org/10.1016/j.jpowsour.2013.10.058.
[30] D.P. Finegan, E. Darcy, M. Keyser, B. Tjaden, T.M.M. Heenan, R. Jervis, J.J. Bailey, R. Malik, N.T. Vo, O.V. Magdysyuk, R. Atwood, M. Drakopoulos, M. DiMichiel, A. Rack, G. Hinds, D.J.L. Brett, P.R. Shearing, Energy Environ. Sci. 10 (2017) 1377–1388, https://doi.org/10.1039/C7EE00385D.
[31] C.J. Orendorff, E.P. Roth, G. Nagasubramanian, J. Power Sources 196 (2011) 6554–6558, https://doi.org/10.1016/j.jpowsour.2011.03.035.
[32] M. Zhang, J. Du, L. Liu, A. Stefanopoulou, J. Siegel, L. Lu, X. He, X. Xie, M. Ouyang, J. Electrochem. Soc. 164 (2017) A3038–A3044, https://doi.org/10.1149/2.0731713jes.
[33] P. Ramadass, W. Fang, Z. Zhang, J. Power Sources 248 (2014) 769–776, https://doi.org/10.1016/j.jpowsour.2013.09.145.
[34] J. Lamb, L.T. Castro. Battery Abuse Testing Manual for Electric and Hybrid Vehicle Applications, 2022. SAND2022-0089 R, https://www.osti.gov/servlets/purl/1838583/.
[35] X. Gao, Y. Jia, W. Lu, Q. Wu, X. Huang, J. Xu, Cell Rep. Phys. Sci. 4 (2023) 101542, https://doi.org/10.1016/j.xcrp.2023.101542.
[36] M.K. Long, S. Liu, G. Zhang, Energy Adv. 2 (2023) 2018–2028, https://doi.org/10.1039/D3YA00311F.
[37] S. Santhanagopalan, P. Ramadass, J. Zhang, J. Power Sources 194 (2009) 550–557, https://doi.org/10.1016/j.jpowsour.2009.05.002.
[38] M. Steinhardt, J.V. Barreras, H. Ruan, B. Wu, G.J. Offer, A. Jossen, J. Power Sources 522 (2022) 230829, https://doi.org/10.1016/j.jpowsour.2021.230829.
[39] M. Keyser, D. Long, A. Pesaran, E. Darcy, M. Shoesmith, B. McCarthy, in: 228th Electrochemical Society (ECS) Meeting, 2015 October 11–15" as ed, 2015. https://www.osti.gov/servlets/purl/1337478. Phoenix, Arizona.
[40] P. Arora, Z. Zhang, Chem. Rev. 104 (2004) 4419–4462, https://doi.org/10.1021/cr020738u.
[41] J. Bai, Z. Wang, D.M. Weragoda, G. Tian, Q. Cai, J. Power Sources 621 (2024) 235293, https://doi.org/10.1016/j.jpowsour.2024.235293.
[42] L. Liu, X. Feng, C. Rahe, W. Li, L. Lu, X. He, D.U. Sauer, M. Ouyang, J. Energy Chem. 61 (2021) 269–280, https://doi.org/10.1016/j.jechem.2021.03.025.